AD-A081 904 AIR FORCE INST OF TECH WRIGHT-PATTERSON AFB OH SCHOO--ETC F/G 11/4
BUCKLING ANALYSIS OF LAMINATED COMPOSITE CIRCULAR CYLINDRICAL S--ETC(U)
DEC 78 J G HARPER
UNCLASSIFIED AFIT/GAE/AA/78D-8 NL

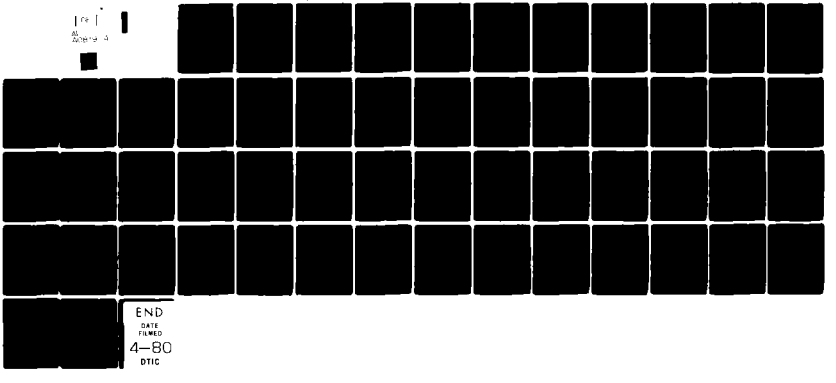

END
DATE FILMED
4-80
DTIC

AFIT/GAE/AA/78D-8

BUCKLING ANALYSIS OF LAMINATED COMPOSITE CIRCULAR CYLINDRICAL SHELLS

THESIS

AFIT/GAE/AA/78D-8 JAMES G. HARPER, II
2Lt USAF

(14) AFIT/GAE/AA/78D-8

(6) BUCKLING ANALYSIS OF LAMINATED COMPOSITE CIRCULAR CYLINDRICAL SHELLS.

THESIS

Presented to the Faculty of the School of Engineering
of the Air Force Institute of Technology
Air University (ATC)
in Partial Fulfillment of the
Requirements for the Degree of
Master of Science

by

James G. Harper, II
2Lt USAF
Graduate Aeronautical Engineering

December 1978

Approved for public release; distribution unlimited.

Preface

I wish to express my extreme gratitude to Dr. Anthony Palazotto for his patience and expert guidance throughout this thesis.

Many thanks to Nick Bernstein and Nick Neigard for their invaluable assistance with STAGS.

To my neglected wife, who I love dearly, I wish to thank for all the love she has given to me.

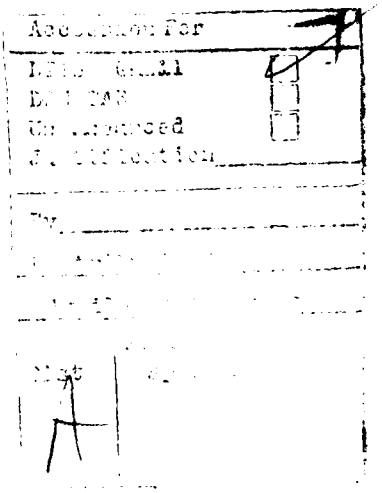

Contents

	Page
Preface	ii
List of Figures	iv
Symbols	v
Abstract	viii
I. Introduction	1
Previous Work	1
Problem Definition	2
Scope	3
II. Theory	6
Bifurcation Buckling	6
Theory of STAGS	8
III. Modeling	15
Boundary Conditions	15
Basic Shell Models	15
Finite Difference Mesh Arrangements	20
IV. Results	22
Shell Buckling Without Prebuckling	22
Prebuckling Effects for Compression	23
Prebuckling Effects for Torsion	26
V. Conclusions	30
Bibliography	32
Appendix A: Series Solutions Without Prebuckling	34
Appendix B: User Problems with STAGS	37
Appendix C: Buckling Loads and Buckling Load Ratios	39
Vita	44

List of Figures

Figure		Page
1	($\pm$ θ, 0°)s Ply Orientation	4
2	Sign Conventions and Notation	5
3	Load-Displacement Curve for Bifurcation	7
4	Clamped Boundary Conditions	16
5	1/8 Shell Model for Axial Compression	18
6	Shell Model for Torsion	19
7	Prebuckling Effect--Axial Compression	24
8	Prebuckling Effect--Torsion, L/R = 7	27
9	Prebuckling Effect--Torsion, L/R = 12	29

Symbols

a	undeformed middle surface radius
a^i	area of i^{th} mesh subregion
A_{ij}	linear (stretching) stiffness matrix
B_{ij}	bending-stretching coupling stiffness matrix
D_{ij}	bending stiffness matrix
D^k	matrix of constants that depend on material properties
E_L	longitudinal modulus of elasticity of fiber
E_T	transverse modulus of elasticity of fiber
F	vector of external forces
F_{cr}	critical load
F_L	linear force vector
G_{LT}	shear modulus
H, h	shell wall thickness
k	mesh station
L	shell length
$L( )$	stiffness operator
$L'( )$	derivative of stiffness operator
M	1/2 sine waves in axial direction
M_x, M_y, M_{xy}	buckling moment resultants
N	sine waves in circumferential direction
N_o	characteristic loading parameter
N_x, N_y, N_{xy}	buckling stress resultants
N_x^i, N_θ^i, $N_{x\theta}^i$	prebuckling membrane force resultants
$N_{x_{SS}}$, $N_{x\theta_{SS}}$	buckling loads determined by series solution

P_b	bifurcation buckling load
$\bar{Q}_{ij}$	transformed reduced stiffness matrix
R	shell radius
S_L^k	vector of linear stress resultants at station k
t	laminate thickness
u, v, w	displacements in x, y, z directions respectively
u^o, v^o	inplane displacements of middle surface
U	strain energy
ΔU^k	strain energy density at station k
V	total potential energy
w,x, w,y	rotations relative to y and x directions respectively
W	work done by external forces
x, y, z	coordinates in axial, circumferential and radial direction respectively
X*	vector of displacement components
X_L	linear solution for a load vector F_L
X_o	solution for a load vector F
Z	layer thickness
Z^{kT}	transpose matrix of strains and curvatures at mesh station k
β	rotation
γ_{LT}	ply shear strain allowable
$\gamma_{x\theta}$	shear strain
ϵ_{ij}	strain tensor
ϵ_L	longitudinal ply strain allowable
ϵ_T	transverse ply strain allowable
θ	ply orientation

κ	curvature
λ	eigenvalue
ν	Poisson's ratio
σ_{ij}	stress tensor
$\tau_{x\theta}$	shear stress

Abstract

The effects of prebuckling displacements on the buckling of laminated composite circular cylindrical shells are investigated. Both axial compression and pure torsion are considered for two shell geometries. A clamped prebuckling boundary condition is used for all analysis with four buckling boundary conditions applied during the buckling process. The shell walls are made up of a 6 ply laminate with several symmetric ply orientations. The study was made using the STAGS computer code, utilizing the linear bifurcation branch with linear prebuckling displacements. The results are compared to the buckling loads determined when prebuckling displacements are neglected. It is shown that prebuckling deformations generally tend to decrease the buckling load of a composite shell. Increased buckling loads can occur under axial compression with prebuckling displacements assumed present, for particular ply orientations, due to a higher bending stiffness. Similarly, under torsion, an increase in buckling load can occur because of a higher tension hoop stress. It is also shown that prebuckling displacements can cause shell buckling before failure of the fibers occurs.

BUCKLING ANALYSIS OF LAMINATED COMPOSITE CIRCULAR CYLINDRICAL SHELLS

I. Introduction

Previous Work

Laminated composite materials, due to their high strength and lightweight properties, are rapidly replacing metals in many structural applications. A widely used structural element, the circular cylindrical shell, is commonly made of various metals for such applications as missile interstage and intertank structures; missile payload, guidance and control adapters; satellite components; and aircraft. Studies have shown Ref (1) that composites reinforced by advanced high modulus fibers such as boron and graphite permit weight savings of 25-40% over competing metallic designs. These advanced composite materials are being used or considered for use in many military and civilian vehicles such as the F-111, F-14, F-15, F-16, F-18, C-5A and space shuttle.

With the high strength and lightweight properties of composites, it can be seen that the detail study of composite cylindrical shells is important. One major area of concern with any structural element is with buckling. Generally, composite shells will have post-buckling strength and integrity, however excessive buckling can lead to failure due to exceeding maximum strain requirements or, if loads are repeated, exceeding the fatigue life. There has been a great deal of work done studying the buckling of isotropic cylindrical shells. Investigations

of how the buckling strength is altered due to variations in the diameter to thickness ratio, length to radius ratio, initial imperfections, prebuckling deformations and buckling boundary conditions for a variety of loading conditions, has been done. For a complete list of references on buckling of isotropic shells, see Reference (2).

Jones and Hennemann (1) investigated the effects of prebuckling deformations on buckling of laminated composite circular cylindrical shells. For a variety of antisymmetric cross ply orientations, they looked at a simply supported edge boundary condition. The effects of prebuckling displacements were found to be negligible for buckling analysis, and they suspected similar results for all other boundary conditions. Further work done on stability of composite shells can be found in References (3)-(9).

Problem Definition

The purpose of this thesis is to investigate how prebuckling displacements effect the buckling of composite shells for two length to radius ratios. Each geometry is studied first under axial compression and then torsion. Along with the geometric instability, a second area investigated is material instability. Different ply orientations for 6 ply laminates are studied to compare buckling loads to composite strengths as estimated from maximum strain criteria. The shell dimensions considered in this thesis are typical of current laboratory tubular specimens presently being tested.

Using classical Fourier analysis in conjunction with Flügge's shell equations modified for anisotropic laminated materials, Whitney

and Sun (10) have obtained buckling loads for the same shells considered in this thesis. The development of these equations is shown in Appendix A. Their results suggest that buckling is a potential problem for tubular specimens. This thesis takes into account prebuckling deformations that Whitney and Sun neglected.

Scope

This thesis looks at two composite circular cylindrical shells, under two independently applied loads, axial compression and pure torsion. Both shells have a 6 ply laminate with $(\pm \theta, 0^{\circ})s$ orientation, illustrated in Figure 1. Computer runs are made for θ ranging from 0° to 90°. The buckling boundary conditions are clamped and summarized as follows:

	$\underline{u}$	$\underline{v}$	$\underline{w}$	$\underline{w,_x}$
CC1	FREE	FREE	0	0
CC2	0	FREE	0	0
CC3	FREE	0	0	0
CC4	0	0	0	0

where u, v and w are displacements in the axial, circumferential and radial directions respectively, as shown in Figure 2. The prebuckling boundary condition used for all cases is CC1. The linear bifurcation branch of the STAGS-C computer code is used, incorporating linear prebuckling deformations.

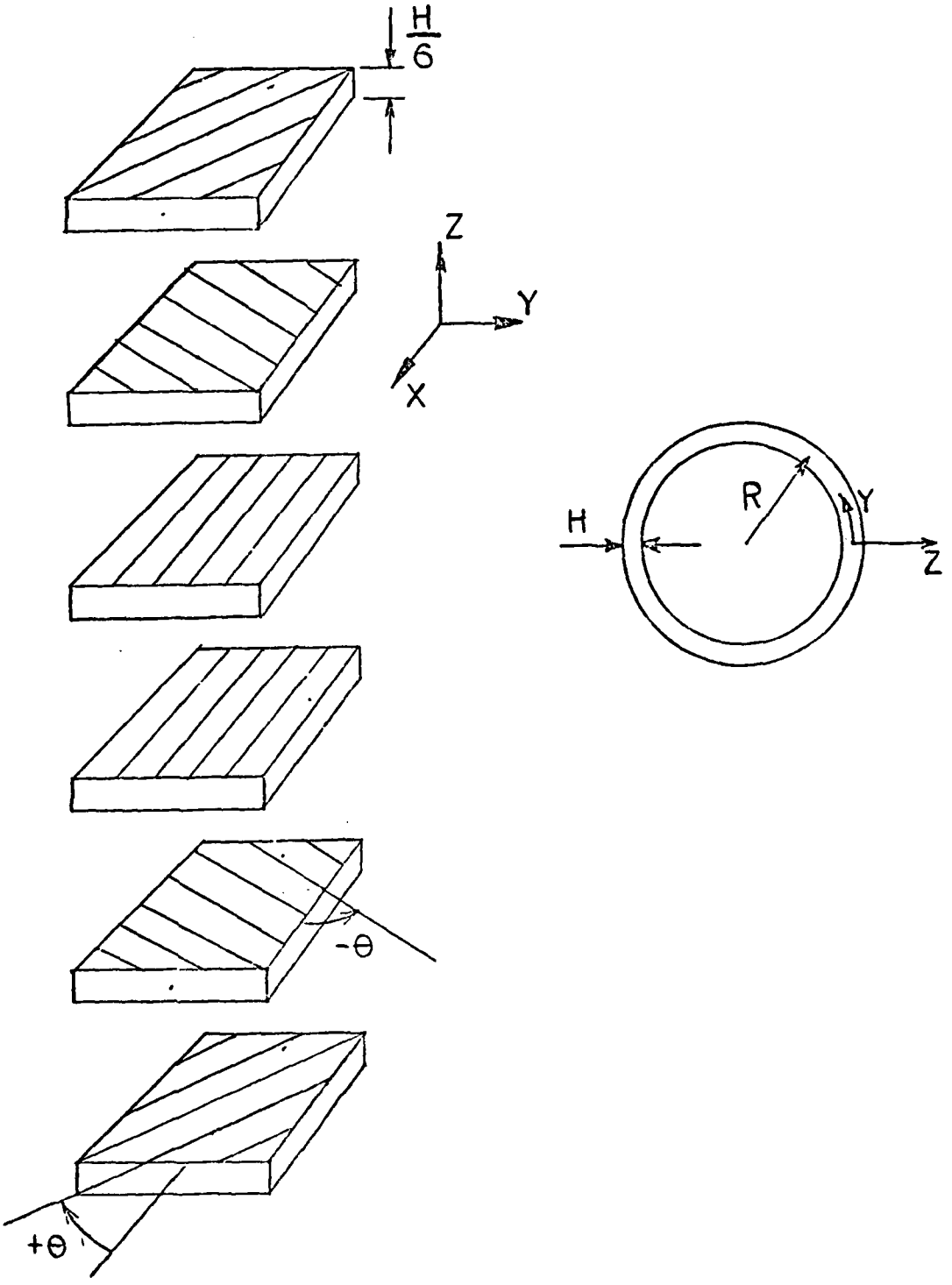

Figure 1. $(\pm \theta, 0^{o})s$ Ply Orientation

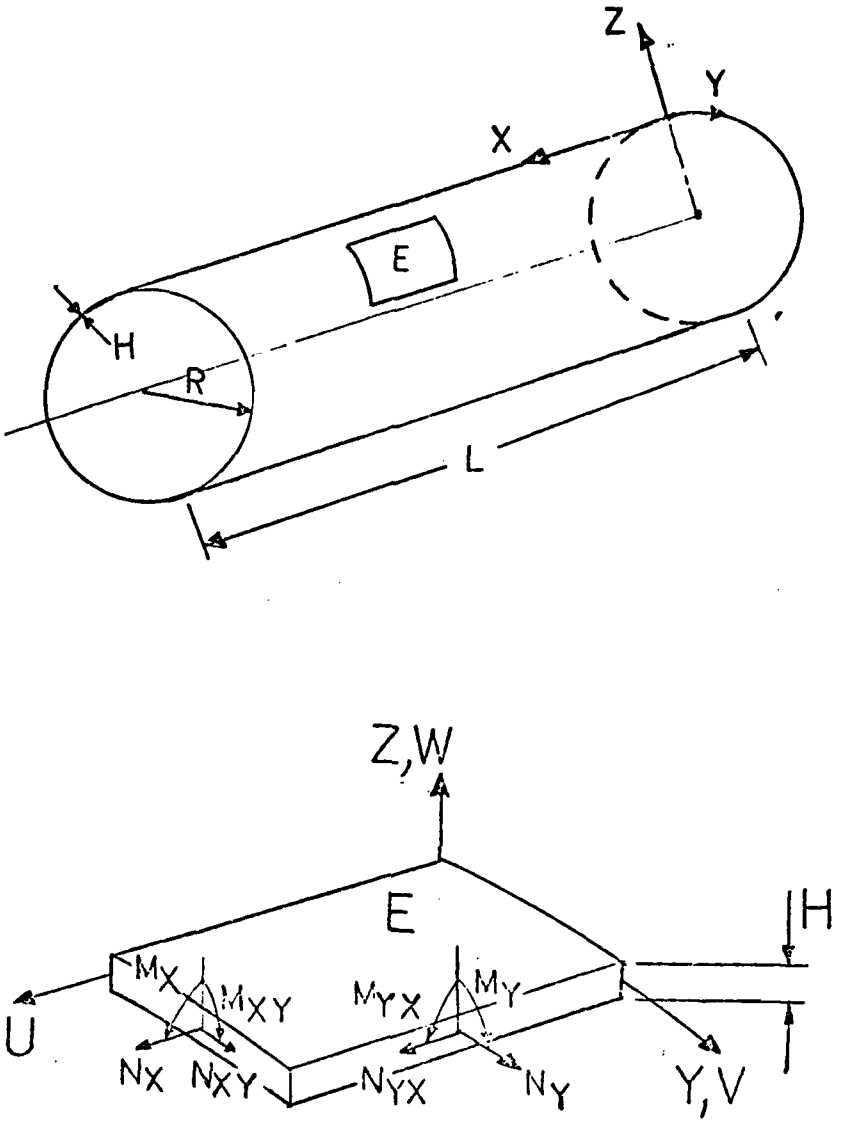

Figure 2. Sign Conventions and Notation

II. Theory

Bifurcation Buckling

Since the linear bifurcation branch of STAGS is used in this investigation, it is appropriate to first discuss the concept of bifurcation buckling. In general, buckling can be defined as a structural deformation due initially to instability under load (Ref 11). It does not matter whether the deformation is elastic or permanent, or whether it leads immediately to collapse or not. For a bifurcation type of buckling, a structure is said to rapidly move from one equilibrium state to another.

Consider the case of the cylindrical shell, subjected to a load P. The load increases monotonically from an initial value of zero. Assume that for sufficiently small values of P, there exists a unique solution to the shell's equilibrium problem. The equilibrium configuration given by this solution is called the primary state or prebuckled state. Then take some value of P, say $P = P_b$, where there exists another equilibrium configuration that is infinitesimally close to the primary state. The existence of two adjacent infinitesimally close equilibrium configurations at the same value of the load $P = P_b$ is called bifurcation, and P_b is called the bifurcation buckling load. This can be illustrated by the curve in Figure 3, in which P is plotted against lateral displacement δ. At each point on the curve an equilibrium configuration exists. The bifurcation point is the point of intersection of the primary path, which starts at the origin and is initially stable, and the secondary

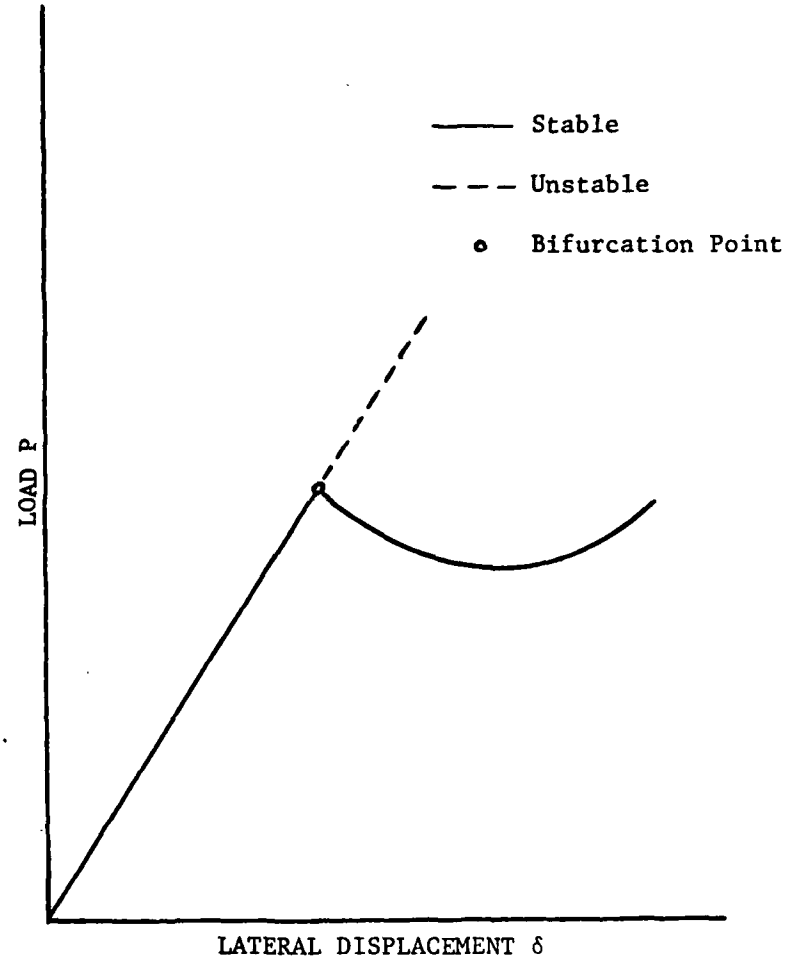

Figure 3. Load-Displacement Curve for Bifurcation

path at $P = P_b$. Since the stability on the primary path is lost above the bifurcation point, the shell will either deform into the equilibrium configuration on the secondary path, or it will be set into motion. The new equilibrium configuration on the secondary (post buckled) path is called the buckled state Ref (12).

The bifurcation buckling load P_b can be determined by different methods. STAGS uses finite-difference approximations of energy equations and solves an eigenvalue problem. This procedure will be described in the section that follows.

Theory of STAGS

STAGS (Structural Analysis of General Shells) is a computer code, developed to analyze general shells under various static, thermal and mechanical loading. The apprcach used by STAGS is a two-dimensional finite difference approximation of energy relations. For this thesis, the problem is for a circular cylindrical shell, with laminated composite fibers oriented in a number of directions. The applied loads are static, and thus the case of static equilibrium must be solved. A necessary condition for static equilibrium is that the total potential energy V, must be stationary, which means the first variation of V is equal to zero. The total potential energy of the shell is equal to the strain energy U, of the shell minus the work done by the external forces W,

$$V = U - W \tag{1}$$

where

$$W = X^* \cdot F$$

X* is the vector of displacement components and F is the vector of external forces.

The strain energy for an orthotropic cylindrical thin shell is given by

$$U = \frac{1}{2} \int \int (\sigma_x \varepsilon_x + \sigma_\theta \varepsilon_\theta + \tau_{x_\theta} \gamma_{x_\theta}) \, dxdy \tag{3}$$

where the strain terms ε_x, ε_θ and γ_{x_θ} are given by

$$\varepsilon_x = u_{,x} + \frac{1}{2} \beta_x^2 \qquad \beta_x = -w_{,x}$$

$$\varepsilon_\theta = \frac{v_{,\theta} + w}{a} + \frac{1}{2} \beta_\theta^2 \qquad \beta_\theta = -\frac{w_{,\theta}}{a} \tag{4}$$

$$\gamma_{x\theta} = \left(\frac{u_{,\theta}}{a} + v_{,x}\right) + \beta_x \beta_\theta$$

The quantities u, v and w are displacement components in the x, θ and directions respectively, and "a" is the undeformed middle surface radius. The stress terms are found by

$$[\sigma_j] = [\bar{Q}_{ij}] [\varepsilon_j] \qquad i,j = 1,2,6 \tag{5}$$

where ε_1, ε_2, ε_6, σ_1, σ_2, and σ_6 are defined as ε_x, ε_θ, $\gamma_{x\theta}$, σ_x, σ_θ and $\tau_{x\theta}$ respectively. The matrix $\bar{Q}_{ij}$ is called the transformed reduced stiffness matrix (see Ref (13) for more detailed analysis of $\bar{Q}_{ij}$).

For the case of the angle ply laminate, the stiffness matrix will be different for each layer. It is therefore necessary to look at the resultant forces and moments acting on the laminate. These are obtained by integrating the stresses in each layer through the

N-layered laminate thickness as follows

$$N_i = \int_{-t/2}^{t/2} \sigma_i dz = \sum_{K=1}^{N} \int_{Z_{K-1}}^{Z_K} \sigma_i dz \qquad i = 1,2,6 \tag{6}$$

and

$$M_i = \int_{-t/2}^{t/2} Z\sigma_i dz = \sum_{K=1}^{N} \int_{Z_{K-1}}^{Z_K} Z\sigma_i dz \qquad i = 1,2,6 \tag{7}$$

Using the relations for the change in curvatures:

$$\kappa_x = \beta_{x,x} \qquad \kappa_\theta = \frac{\beta_{\theta,\theta}}{a}$$

$$\kappa_{x\theta} = \frac{1}{2}\left(\frac{\beta_{x,\theta}}{a} + \beta_{\theta,x} \right) \tag{8}$$

and combining this with Eqs (4) and (5), Eqs (6) and (7) become in matrix form

$$\begin{bmatrix} N_i \\ M_i \end{bmatrix} = \begin{bmatrix} A_{ij} & B_{ij} \\ B_{ij} & D_{ij} \end{bmatrix} \begin{bmatrix} \varepsilon^o{}_j \\ \kappa_j \end{bmatrix} \qquad i,j = 1,2,6 \tag{9}$$

where the stretching, bending-stretching coupling, and bending stiffness submatrices are defined as

$$(A_{ij},\ B_{ij},\ D_{ij}) = \int_{-t/2}^{t/2} (1,\ Z,\ Z^2)\ \bar{Q}_{ij} dz \tag{10}$$

For the shell that is laminated symmetrically with respect to the middle surface, as is the case in this thesis, the bending-stretching submatrix B_{ij} equals zero. This yields the following expressions for middle surface strains

$$\{\varepsilon_j{}^o\} = [\, A_{ij} \,]^{-1} \{N_i\} \tag{11}$$

and curvatures

$$\{\kappa_j\} = \left[D_{ij} \right]^{-1} \{M_i\} \tag{12}$$

With the middle surface strains and curvatures, the total strains at an arbitrary distance z from the middle surface are

$$\epsilon_j = \epsilon_j^{\,o} + z\kappa_j \qquad j = 1,2,6 \tag{13}$$

Using Eqs (13) and (5), all the terms in the strain energy are now known. In order to approximate the strain energy and thus the total potential energy, STAGS models the shell structure by placing mesh lines paralled to the x and y coordinate lines. The intersection of these mesh lines represent nodes or mesh stations i, and the area bounded by mesh lines would be a; the area of the i^{th} subregion. The total strain energy would then be given by

$$U = \sum_{i}^{M} \Delta u^i \cdot a^i \tag{14}$$

where M is the number of mesh stations and Δu^i, which is the integrand of Eq (3), is the strain energy density at mesh station i. With the work W, and strain energy U, now given in terms of the unknown displacements, STAGS replaces finite difference approximations for those displacements in the total potential energy V, given by Eq (1).

As previously stated, for the condition of stationary potential energy, the first variation must vanish. This leads to the equation

$$LX = F \tag{15}$$

where L is a stiffness operator which relates displacement components and external forces, and is defined as

$$LX = \text{GRAD } U \tag{16}$$

Since only the linear terms are included in the deformations of strain and curvature, then for linear bifurcation theory, L is a linear operator represented in matrix form.

For the bifurcation problem let X_o be a solution of Eq (15) for a given external force vector F. If another displacement vector Y, in every neighborhood of X_o satisfies the equation

$$LY = F \tag{17}$$

then bifurcation is said to take place for the shell under load F. Since Eq (15) can have multiple solutions, a necessary condition for bifurcation required that L'_{X_o}, which is the derivative of the stiffness operator, be a singular matrix. This leads to

$$\det (L'_{X_o}) = 0 \tag{18}$$

from which classical bifurcation theory may be obtained. It is then assumed that X_o may be written as

$$X_o = \lambda X_L \tag{19}$$

where X_L is the linear solution for a load vector F_L. Thus Eq (18) becomes

$$\det (L'_{\lambda X_L}) = 0 \tag{20}$$

Eq (20) represents an algebraic eigenvalue problem. Omitting the nonlinear prebuckling rotations for linear bifurcation theory, Eq (20) becomes

$$\det (A - \lambda D) = 0 \tag{21}$$

this leads to the following eigenvalue problem

$$AX = \lambda DX \tag{22}$$

where A is the linear stiffness matrix, and D is the bending stiffness matrix. Briefly, the formation of the A and D matrix is as follows. Consider the stiffness operator derivative L'_{X_o}, which represents the coefficient matrix for the linear system of governing algebraic equations where the nodal displacements are the unknowns. The elements of L'_{X_o} are given by

$$L'_{i,j} = \frac{\partial^2 U}{\partial X_i \partial X_j} \tag{23}$$

Applying Eq (23) to Eq (14) yields

$$\frac{\partial^2 U}{\partial X_i \partial X_j} = \sum_{k=1}^{M} a^k \frac{\partial^2 \Delta U^k}{\partial X_i \partial X_j} \tag{24}$$

The strain energy density ΔU^k can be written

$$\Delta U^k = Z^{kT} D^k U^k \tag{25}$$

where the matrix Z^k represents the strains and curvatures at mesh station k and D^k is a matrix of constants that depend on the material properties. Recall the integrand of Eq (3) is the strain energy

density for the cylindrical shell. The vector of linear stress resultants at station k is defined as

$$S_L{}^k = D^k Z^k \tag{26}$$

Incorporating Eqs (25) and (26) together, the k^{th} term of Eq (24) is

$$\frac{\partial^2 \Delta U^k}{\partial x_i \partial x_j} = \frac{\partial^2 Z^{kT}}{\partial x_i \partial x_j} \lambda S_L{}^k + \frac{\partial Z^{kT}}{\partial X_i} D^k \frac{\partial Z^k}{\partial X_j} \tag{27}$$

For the case of neglected prebuckling notations, the last term of Eq (27) generates the linear stiffness matrix A. The first term of Eq (27) contributes to the bending stiffness matrix D. The critical load F_{CR} is determined when the smallest eigenvalue λ is found that satisfies Eq (21). The critical load is a multiple of the linear force vector F_L

$$F_{CR} = \lambda F_L \tag{28}$$

Ref (14) shows a more detailed analysis of the eigenvalue problem.

III. Modeling

Boundary Conditions

There are four clamped boundary conditions used in this thesis referred to as CC1, CC2, CC3 and CC4 (see Fig 4 for a physical representation). Rollers allow freedom of movement while flanges restrict displacement perpendicular to the plane of the flange. Due to the restraining moments of a clamped condition the slope $w,_x$ is zero at the shell boundary. Notice also that the displacement w, is zero at the boundary for all four cases.

STAGS models these four boundary conditions by allowing or restraining the particular displacements. The $N_x = 0$ and $N_{xy} = 0$ conditions are specified by allowing u and v respectively to be free. The $u = 0$, $v = 0$, $w = 0$, and $w,_x = 0$ restraints are specified directly by setting the appropriate edge quantity to zero. STAGS also has several built-in boundary conditions. One of them was used in this thesis, referred to as symmetry. Symmetry means that a boundary lying along the y or circumferential direction has $u = w,_x = 0$, and a boundary lying along the x or axial direction has $v = w,_y = 0$. See Fig 5.

Basic Shell Models

As previously stated, there are two L/R ratios studied in this thesis. Each shell geometry has a radius (R) of 5.25" and a thickness (h) of .5". The L/R ratios considered are 12 and 7, yielding a length (L) of 63" and 36.75" respectively. For each shell there are two loading arrangements applied independently, axial compression and

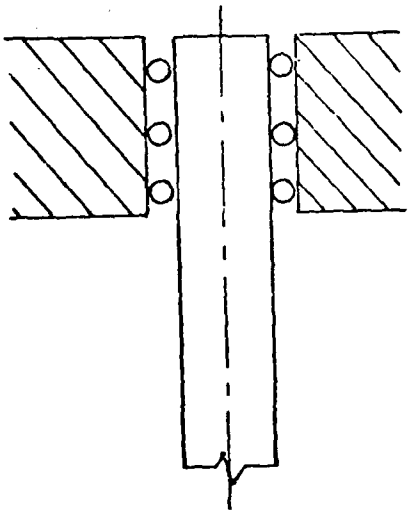

CC1

$w = 0 \quad w_{,x} = 0 \quad N_x = 0 \quad N_{xy} = 0$

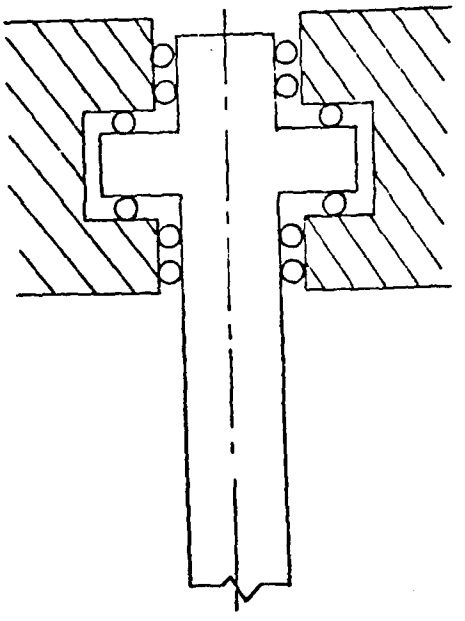

CC2

$w = 0 \quad w_{,x} = 0 \quad u = 0 \quad N_{xy} = 0$

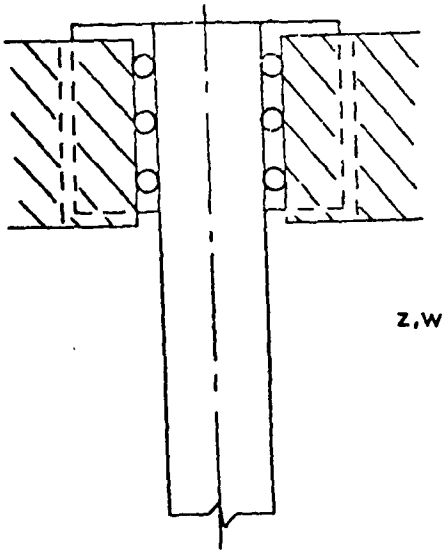

CC3

$w = 0 \quad w_{,x} = 0 \quad N_x = 0 \quad v = 0$

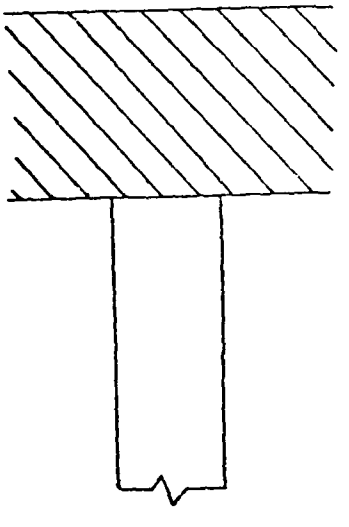

CC4

$w = 0 \quad w_{,x} = 0 \quad u = 0 \quad v = 0$

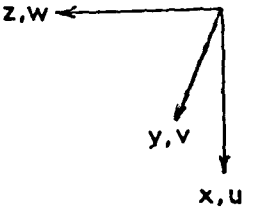

Figure 4. Clamped Boundary Conditions (from Ref (15))

torsion. Due to the nature of the loads, the shell model for each load was different and will now be presented.

For the case of axial compression, a constant line load was applied to the shell. Due to the symmetry of the loaded shell, only 1/8 of the shell was modeled. The only difference between the model for L/R = 12 and L/R = 7 is the value of L/2 (see Fig 5). The boundary condition for each boundary, as seen in Fig 5, is as follows: For boundary 1, which is the top of the shell, the conditions are specified according to the particular boundary condition being investigated. All prebuckling boundary conditions are CC1, and buckling boundary conditions are CC1, CC2, CC3 and CC4. Boundaries 2, 3, and 4 are considered to be symmetry.

For the case of torsion, due to the fact that symmetry of displacement is not present, the whole shell had to be modeled (see Fig 6). A problem arose that indicated a rigid body mode, and thus it became necessary to improve the model. It was determined that fixing the circumferential displacement v, of at least one node on a boundary would alleviate the rigid body problem. Some sample runs indicated that holding all the nodes of one edge fixed in the v direction made for a better model than just fixing one node. This was taken care of for that edge by letting v = 0 in the boundary conditions. Also, no shear for that edge was applied since it was fixed in the circumferential direction, which yields the same as applying the shear (see Appendix B).

For L/R = 7, the shear was applied to the top edge. The boundary conditions for the top and bottom edge were the same conditions used

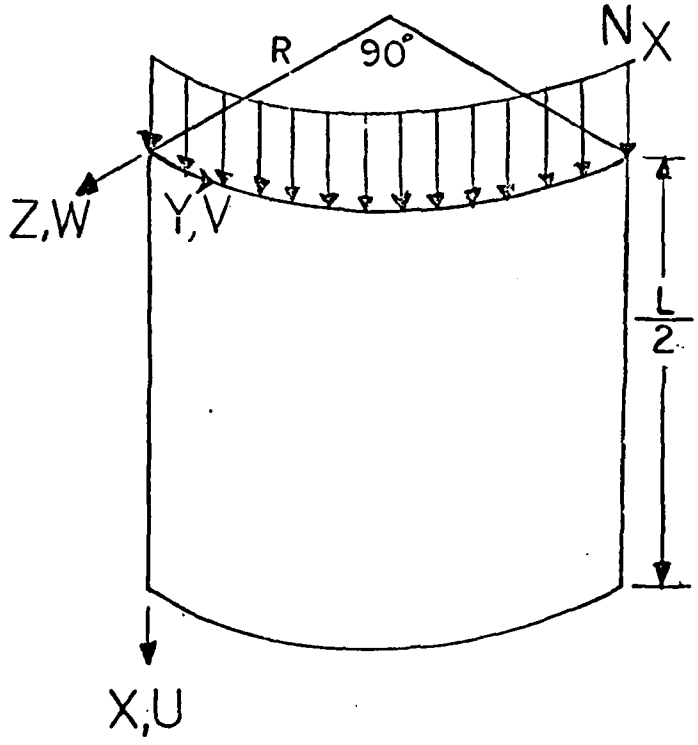

Figure 5. 1/8 Shell Model for Axial Compression

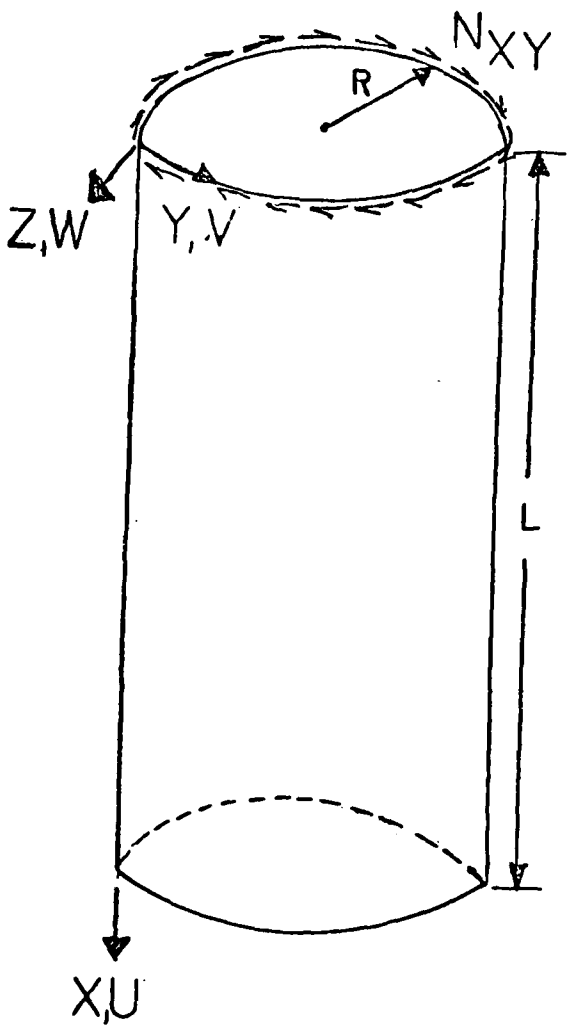

Figure 6. Shell Model for Torsion

in axial compression, CC1 prebuckling and CC1 through CC4 buckling. The only difference being the added constraint of v = 0 along the bottom edge. What were called boundaries 2 and 4 for the 1/8 shell model, are not really boundaries for the whole shell. There is an option in STAGS that allows two boundaries to have compatible displacements, since there must be an allowance for four boundaries. This option takes care of the treatment of the whole shell.

The L/R = 12 geometry had the same model with the exception of a different mesh size. The mesh sizes will be discussed in the section that follows.

Both shells considered were made of graphite/epoxy composites, with the following material properties

$$E_L = 20 \times 10^6 \text{psi},\ E_T = 10^6 \text{psi},\ G_{LT} = 0.6 \times 10^6 \text{psi},\ \nu_{LT} = 0.25$$

where L denotes the direction parallel to the fibers, T denotes the direction transverse to the fibers, and ν_{LT} is the Poisson ratio as determined from a tensile test parallel to the fibers (Ref 10).

The laminates for each shell were 6 ply and oriented by $(\pm \theta, 0^\circ)s$. θ was 0°, 15°, 30°, 45°, 60°, 75° and 90°.

Finite Difference Mesh Arrangements

There were four different mesh arrangements used in this thesis. For the 1/8 shell model, 210 nodes at a mesh size of .92" x .92" were used for the L/R = 7, and 340 nodes at a mesh size of .92" x .95" for L/R = 12. An attempt to test the accuracy obtained by these mesh sizes was made by tripling the number of nodes (which almost tripled the

computer cost). This smaller mesh size gave a higher buckling load of less than only 1.5% which, for the additional cost, is an insignificant increase in accuracy. Decreasing the number of nodes by 30% gave only 2 or 3 nodes per 1/2 sine wave. It was felt that 5 or 6 nodes per 1/2 sine wave were necessary for any accuracy Ref (15), and this was achieved by the aforementioned mesh arrangements.

For the whole shell model, a problem of ill-conditioned variables arose for both geometries. The L/R = 7 case was modeled with 1054 nodes giving a mesh size of 1.11" x 1.06". This mesh arrangement was used for all angles except $\theta = 0^{\circ}$. At $\theta = 0^{\circ}$, ill-conditioned variables in the stiffness matrix caused the matrix decomposition to be discontinued prematurely (see Appendix B). This was a problem for angles θ, less than 8°. At 8°, the analysis was successful, and from this and other results, the buckling load at $\theta = 0^{\circ}$ was extrapolated. The L/R = 12 model initially had 989 nodes at a mesh size of 1.47" x 1.50", but this mesh arrangement yielded ill-conditioned stiffness matrix for most all angles of θ. The number of nodes was increased to 1128 giving a mesh size of 1.37" x 1.37". The latter arrangement worked for all angles θ except 0°. The identical procedure used in obtaining the buckling load at $\theta = 0^{\circ}$ for L/R = 7, was used here for L/R = 12.

IV. Results

Shell Buckling Without Prebuckling

The problem of determining the buckling load for a composite cylindrical shell, without taking into account the prebuckling deformations, can be done by using a series solution. This approach was taken for an L/R = 12, by Whitney and Sun (10), for both axial compression and torsion, and is given in Appendix A.

Whitney and Sun took the buckling loads, obtained by the series solution, and normalized them for specific ratios of L/R and R/h. This was done by dividing the buckling load by the product of transverse modulus of elasticity of the fibers E_T, and shell wall thickness h. This normalized load would then hold for any shell of length L, radius R, and thickness h, provided the ratios of L/R and R/h remained the same. The normalized loads were then plotted against the ply orientations θ. Included in the graphs were an estimated strength based on maximum strain criterion, as presented by Petit and Waddoups (16). Ply strain allowables chosen for the maximum strain criterion were

$$\varepsilon_L^+ = 0.01 \text{ in/in} \qquad \varepsilon_L^- = 0.008 \text{ in/in}$$

$$\varepsilon_T^+ = 0.004 \text{ in/in} \qquad \varepsilon_T^- = 0.01 \text{ in/in}$$

$$\gamma_{LT} = 0.015 \text{ in/in}$$

where + denotes tension and - denotes compression. The graphs described above, for the ply orientation $(\pm \theta, 0^\circ)$s, have been

reproduced in Figs 7-9. Simple comparisons can then be made to the buckling of shells when prebuckling deformations are included. The following sections will describe the effects of prebuckling.

Prebuckling Effects For Compression

As previously stated, CC1 prebuckling boundary conditions were used in all test cases. Starting with the shell having L/R = 12, runs were made at each angle θ for CC1 buckling boundary conditions. The results showed that for $\theta = 0^{\circ}$, there was a 22% drop in the buckling load from the series solution with no prebuckling. For all other ply orientations, the buckling load ranged from 2% to 12% of a decrease from the series solution. The buckling loads for CC3 buckling turned out to be almost identical to the loads found for CC1, all within 3%. This similarity is not unexpected since in both cases, the axial displacement is allowed to move freely. Fig 7 shows the comparison of the buckling loads determined from the series solution, and the buckling loads calculated where prebuckling is considered. Appendix C shows the results in tabular form.

For both CC2 and CC4 conditions, the buckling loads were also nearly identical, and for ply orientations except $\theta = 15^{\circ}$, the loads were the same as for CC1 and CC3. For $\theta = 15^{\circ}$, however, an increase in the buckling load of approximately 10% over the series solution was found. That is nearly 20% higher than the value expected from other observed cases. Attempts to insure that the increase was not caused by a poor model were made. Steps to check the model included the following; increasing the load by 50%, increasing the number of nodes

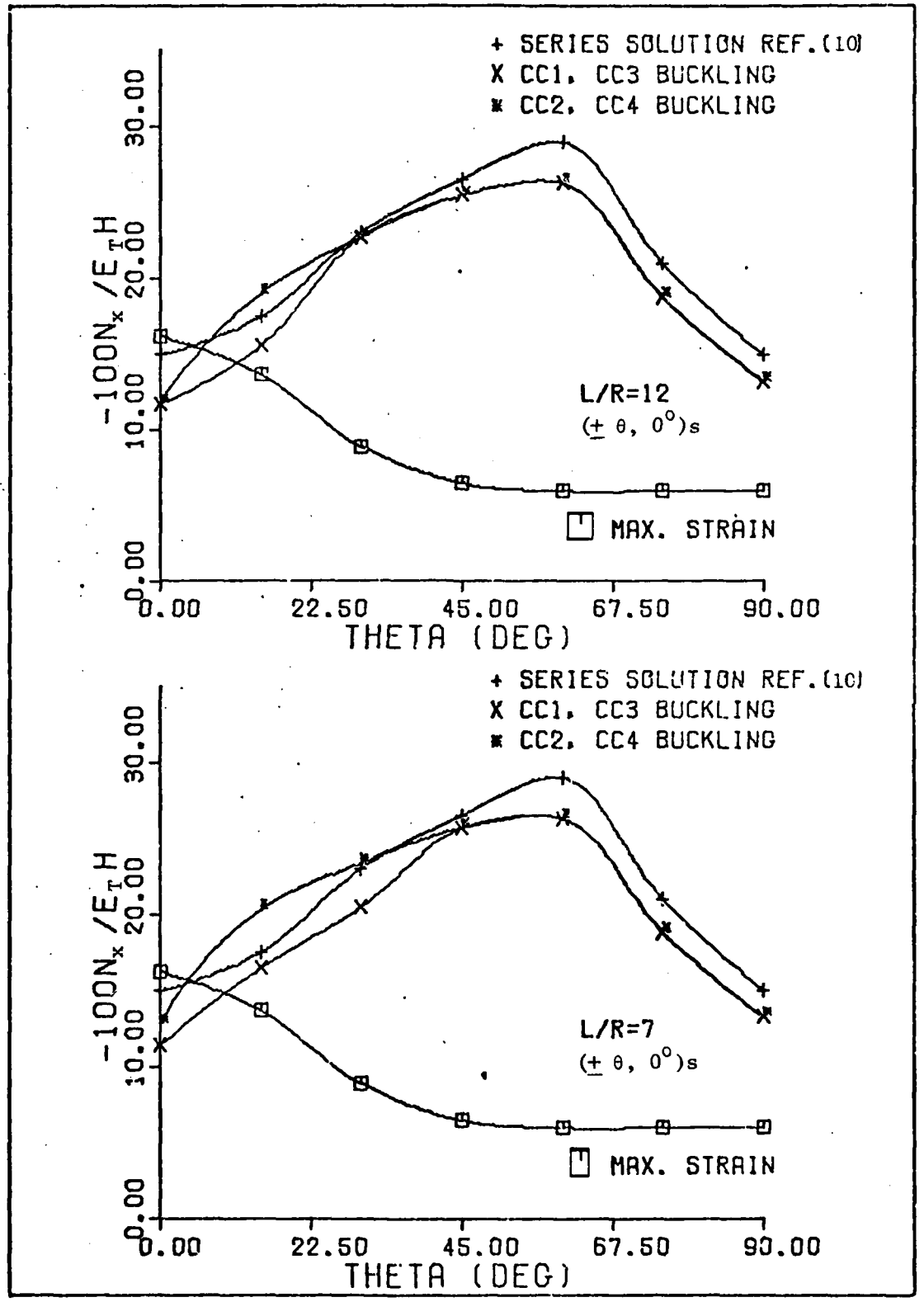

Figure 7. Prebuckling Effect - Axial Compression

by 30% and modeling the entire shell with 989 nodes and a mesh size of 1.47" x 1.50". In all three cases the buckling load remained the same for $\theta = 15^{\circ}$.

Once it became apparent that the model was good, it became necessary to explain why the shell, at the angle $\theta = 15^{\circ}$, was stiffer than for the case of neglected prebuckling displacements. Investigation of the prebuckling moments, showed that for $\theta = 15^{\circ}$, the values of M_x were higher than for other ply orientations. With the case where no prebuckling deformation is considered, the only load is the applied load N_x, and so other prebuckling forces and moments, including M_x, are zero. Taking into account the prebuckling forces and moments, which arise when prebuckling displacements are considered, the substantially larger M_x for $\theta = 15^{\circ}$ makes for a relatively higher bending stiffness than for other ply orientations. This relatively higher bending stiffness, which will resist buckling when the load was in the axial direction, makes for a higher buckling load relative to the case where no prebuckling displacement is considered.

Test runs made for the L/R = 7 case were made for the same boundary conditions and ply orientations. It was found that all comparisons made for L/R = 12, were similar to those for L/R = 7. The only difference was that the increased buckling load found at $\theta = 15^{\circ}$ for L/R = 12, was true for both $\theta = 15^{\circ}$ and $\theta = 30^{\circ}$ for L/R = 7. The prebuckling M_x was higher for both angles as well, and therefore the same conclusions are drawn. It was also shown that the change in buckling load due to a different L/R ratio was very small (see Fig 7), except at $\theta = 15^{\circ}$ and $\theta = 30^{\circ}$. It can therefore be

concluded that the boundary effect is very slight except at $\theta = 15^{\circ}$ and 30°.

It became apparent that for both shell geometries, the significant buckling constraint is $u = 0$. It is when the axial displacement on the boundary is held fixed at buckling after it is allowed to move freely in prebuckling that the variation from series solutions is obtained.

Comparisons can also be made between the buckling loads and composite strength, as estimated from maximum strain criterion. For certain small angles θ, the curve for CC1 and CC3 buckling remain under the maximum strain curve, where for the same θ for the series solution is above (see Fig 7).

Prebuckling Effects For Torsion

The prebuckling and buckling boundary conditions used for torsion were the same as with axial compression. It was found, as was the case with axial compression, that for CC1 and CC3 conditions, the buckling loads were the same. Similarly with CC2 and CC4.

For cases of $L/R = 7$ under torsion the values of buckling loads shown in Fig 8 are higher than the series solution, ranging from 15%-28% (recall that the series solution is done for $L/R = 12$), which only indicates that a shorter shell demands a greater applied twist to buckle. The shell length played more of a role in the case of torsion than it did with axial compression, where very little change in buckling load occurred due to the change in length (see Figs 7 and 8).

The final investigation was for an $L/R = 12$ under torsion. It

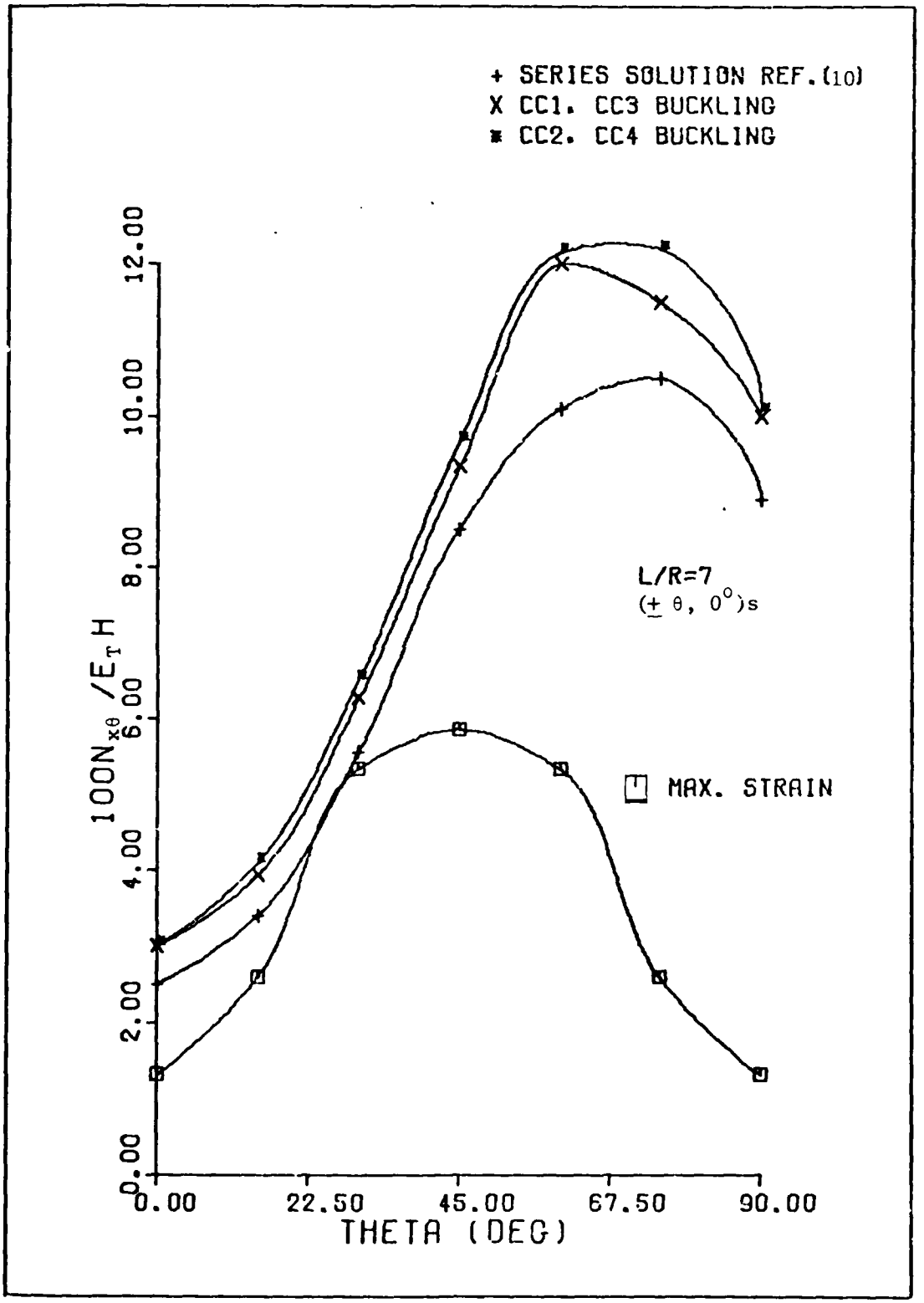

Figure 8. Prebuckling Effect - Pure Torsion

was found that for angles of $\theta = 75^{\circ}$ and below, the buckling loads ranged from 6% to 12% below the series solution, for CC2 and CC4 buckling. For CC1 and CC3 buckling the drop ranged from 9% to 22% (see Fig 9). At $\theta = 90^{\circ}$ for all four boundary conditions, the buckling load was approximately 8% higher than the series solution. Investigation of the prebuckling stresses showed that there is more tension in the hoop (v) direction at $\theta = 90^{\circ}$, than for all other angles of θ. The tension stress, along with the greater hoop stiffness comes about because the torsion stress field acts over a larger area in v direction for ply orientation $\theta = 90^{\circ}$. This is true because the ply orientation of 90° is parallel to the v direction. The tension stress acts to resist torsion buckling and so this added resistance that is not as great as for other ply angles θ, has the effect of increasing the buckling load relative to the series solution.

Comparing the two L/R ratios for the case of torsion, it is shown that for $\theta > 45^{\circ}$ there is a marked difference in the shape of the curves. For L/R = 7, the maximum buckling load occurs at around $\theta = 60^{\circ}$, the curve then begins to drop off as the boundary conditions come in to play. For L/R = 12, the curve flattens out at $\theta > 75^{\circ}$ because of the increase in tension hoop stress.

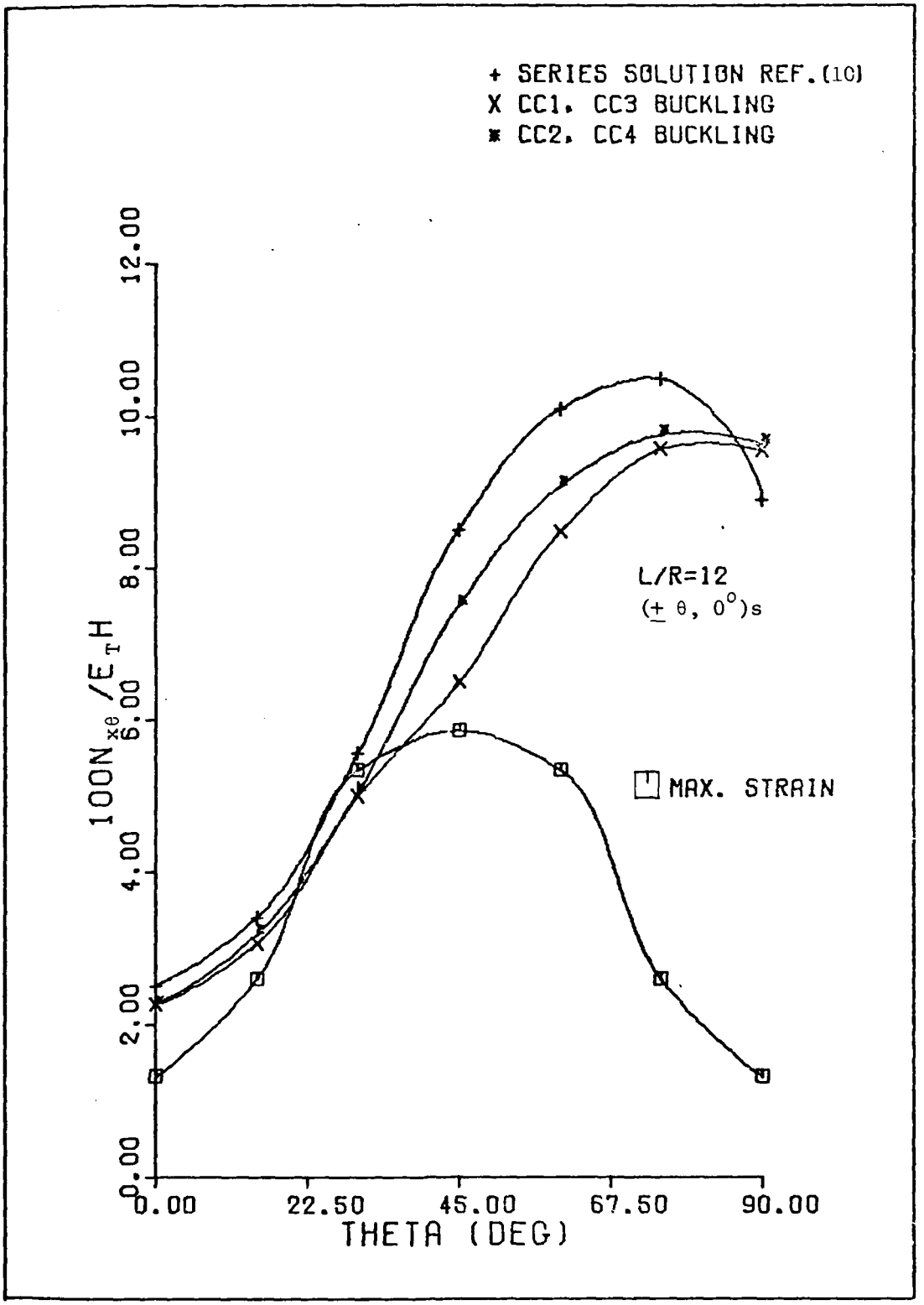

Figure 9. Prebuckling Effect - Pure Torsion

V. Conclusions

From the results generated in this thesis, several conclusions can be drawn concerning the prebuckling effects of composite shells, with ply orientation of $(\pm \theta, 0^{\circ})s$, under axial compression and torsion.

1) Under axial compression and torsion, prebuckling deformations generally tend to reduce the buckling load of composite shells.

2) For certain ply orientations, the prebuckling effects can increase the buckling load.

3) For a shell under axial compression, the $u = 0$ constraint in buckling is the important factor in determining the prebuckling effects.

4) A change in length of a composite shell affects the buckling load much more under torsion than for compression, as is consistent with isotropic shells.

5) For both axial compression and torsion, the buckling boundary conditions CC1 and CC3 act nearly the same while CC2 and CC4 act similarly.

6) For small ply angles θ, under axial compression, the effects of prebuckling displacement can cause buckling before failure of the fibers occurs, based on maximum strain criterion. This is also true under torsion, for angles θ from about 25° to 35°.

7) A higher prebuckling bending stiffness for a particular ply orientation, under axial compression, has the effect of increasing the buckling load over that of the solution generated with prebuckling neglected.

8) A greater prebuckling tension stress can cause, for 90° oriented fibers, a higher buckling load under applied torsion, than the load determined when no prebuckling is considered.

9) For the case of torsion, the boundary conditions have greater affect on the shell with L/R = 7 than with L/R = 12.

Bibliography

1. Jones, R. M., and Hennemann, J. C. "Effect of Prebuckling Deformations on Buckling of Laminated Composite Circular Cylindrical Shells." AIAA 19th Structures, Structural Dynamics and Materials Conference, Bathesda, Maryland. 78-516, April 3-5, 1978.

2. Brush, D. O., and Almroth, B. O. Buckling of Bars, Plates, and Shells. New York: McGraw-Hill, 1975.

3. Pagano, N. J., and Whitney, J. M. "Geometric Design of Composite Cylindrical Characterization Specimens." Journal of Composite Materials 4:360-378 (July 1970).

4. Pagano, N. J. "Stress Gradients in Laminated Composite Cylinders." Journal of Composite Materials 5:260-265 (April 1971).

5. Whitney, J. M. "On the Use of Shell Theory for Determining Stresses in Composite Cylinders." Journal of Composite Materials 5:340-353 (July 1971).

6. Marlowe, D. E., Sushinsky, G. F., and Dexter, H. B. "Elastic Torsional Buckling of Thin-Walled Composite Cylinders." Composite Materials: Testing and Design (Third Conference). ASTM STP 546, American Society for Testing and Materials, 84-108, 1974.

7. Jones, R. M., and Morgan, H. S. "Buckling and Vibration of Cross-Ply Laminated Circular Cylindrical Shells." AIAA Journal, 664-671 (May 1975).

8. Stein, M. The Influence of Prebuckling Deformations and Stresses on the Buckling of Perfect Cylinders. NASA Technical Report R-190. Washington: National Aeronautics and Space Administration, February, 1964.

9. Almroth, B. O. "Influence of Edge Conditions on the Stability of Axially Compressed Cylindrical Shells." AIAA Journal, 134-140 (January 1966).

10. Whitney, J. M., and Sun, C. T. "Buckling of Composite Cylindrical Characterization Specimens." Journal of Composite Materials, 9:138-148 (April 1975).

11. Nayler, J. L. Dictionary of Aeronautical Engineering. Totowa, N.J.: Littlefield, Adams and Co., 1967.

12. Sobel, L. H. On the Basic Concepts of the Instability of Structures. U.S. Atomic Energy Commission Contract Report E(11-1) -3045. September, 1976.

13. Jones, R. M. Mechanies of Composite Materials. New York: McGraw-Hill, 1975.

14. Almroth, B. O., et al. "User's Manual for the STAGS-A Computer Code." Collapse Analysis for Shells of General Shells, Vol. II. AFFDL TR-71-80. WPAFB, Ohio; Air Force Flight Dynamics Laboratory, March, 1973.

15. Nelson, Capt. D. A. "Buckling of Axially Compressed Stringer Stiffened Cylindrical Shells With and Without Cutouts." Master's Thesis, Air Force Institute of Technology. WPAFB, Ohio, December, 1977.

16. Petit, P. H., and Waddoups, W. E. "A Method of Predicting the Nonlinear Behavior of Laminated Composites." Journal of Composite Materials, 3:2 (January 1969).

17. Flügge, W. Stresses in Shells. Berlin: Springer-Verlag, 1960.

18. Cheng, S., and Ho, B. P. C. "Stability of Heterogeneous Aeolotropic Cylindrical Shells Under Combined Loading." AIAA Journal, 1:892-898 (April 1963).

Appendix A

Series Solution Without Prebuckling

The buckling problem of a composite cylindrical shell was solved by Whitney and Sun (10). They used classical Fourier analysis in conjunction with Flügge's shell equations modified for anisotropic laminated materials. Parts of the development will be shown here to briefly outline the procedure. For the complete analysis, see Reference (10).

Consider a laminated cylindrical shell of wall thickness h with a middle surface radius of R. The coordinate system is in the middle surface with x, θ and z measured along the longitudinal, circumferential, and radial direction, respectively. Denoting partial differentiation by a comma, the governing equations for the static stability analysis of laminated anisotropic cylindrical shells based on Flügge's theory (17) are of the form (18)

$$L_{11}u^\circ + L_{12}v^\circ + L_{13}w + N_x^i u^\circ_{,xx} + \frac{N_\theta^i}{R}\left(\frac{u^\circ_{,\theta\theta}}{R} - w_{,x}\right) + 2\frac{N_{x\theta}^i}{R}u^\circ_{,x\theta} = 0 \tag{A1}$$

$$L_{12}u^\circ + L_{22}v^\circ + L_{23}w + N_x^i v^\circ_{,xx} + \frac{N_\theta^i}{R^2}(w_{,\theta} + v^\circ_{,\theta\theta}) + 2\frac{N_{x\theta}^i}{R}(w_{,x} + v_{,x\theta}) = 0 \tag{A2}$$

$$L_{13}u^\circ + L_{23}v^\circ + L_{33}w - N_x^i w_{,xx} - \frac{N_\theta^i}{R}\left(u^\circ_{,x} - \frac{v^\circ_{,\theta}}{k} + \frac{w_{,\theta\theta}}{R}\right) - 2\frac{N_{x\theta}^i}{R}(w_{,x\theta} - v^\circ_{,x}) = 0 \tag{A3}$$

where u° and v° are the inplane displacements of the middle surface in the x and θ directions, respectively, w is the transverse displacement of the middle surface, and N_x^i, N_θ^i and $N_{x\theta}^i$ are initial (pre-buckling)

membrane force resultants defined in the usual manner. Looking at three of the six operators L_{ij}, gives an indication of the complexity of the problem. The L_{ij} operators are defined for symmetric laminates.

$$L_{11} = A_{11}(\ )_{,xx} + 2\frac{A_{16}}{R}(\ )_{,x\theta} + \frac{A_{66}}{R^2}(\ )_{,\theta\theta} \tag{A4}$$

$$\begin{aligned} L_{13} = &-\frac{D_{11}}{R}(\ )_{,xxx} - \frac{D_{16}}{R^2}(\ )_{,xx\theta} + \frac{D_{66}}{R^3}(\ )_{,x\theta\theta} \\ &+ \frac{D_{26}}{R^4}(\ )_{,\theta\theta\theta} + \frac{A_{12}}{R}(\ )_{,x} + \frac{1}{R^2}\left(A_{26} + \frac{D_{26}}{R^2}\right)(\ )_{,\theta} \end{aligned} \tag{A5}$$

$$\begin{aligned} L_{33} = &D_{11}(\ )_{,xxxx} + 4\frac{D_{16}}{R}(\ )_{,xxx\theta} + \frac{2}{R^2}(D_{12} + 2D_{66})(\ )_{,xx\theta\theta} \\ &+ 4\frac{D_{26}}{R^3}(\ )_{,x\theta\theta\theta} + \frac{D_{22}}{R^4}(\ )_{,\theta\theta\theta\theta} - 2\frac{D_{26}}{R^3}(\ )_{,x\theta} \\ &+ 2\frac{D_{22}}{R^4}(\ )_{,\theta\theta} + \frac{1}{R^2}\left(A_{22} + \frac{D_{22}}{R^2}\right)(\ ) \end{aligned} \tag{A6}$$

where A_{ij} and D_{ij} are the inplane stiffness matrix and bending stiffness matrix, respectively which are defined in Eq. (10). In the present analysis, initial loads are constant and of the form $N_x^i = k$, N_o, $N_\theta^i = k_2 N_o$, and $N_{x\theta}^i = k_3 N_o$, where k_i are prescribed constants, and N_o is a characteristic loading parameter.

CC4 boundary conditions were assumed for the buckling solution (recall that prebuckling displacements were neglected), which means

$$\begin{aligned} &u^\circ(0,\theta) = v^\circ(0,\theta) = w(0,\theta) = w_{,x}(0,\theta) \\ &= u^\circ(L,\theta) = v^\circ(L,\theta) = w(L,\theta) = w_{,x}(L,\theta) = 0 \end{aligned} \tag{A7}$$

where L denotes cylinder length. A solution to Eqs. (A1) - (A3) is a Fourier series.

The displacementsw becomes

$$\begin{aligned} w = &\sin n\theta \sum_{m=1}^{\infty} F_{mn} \sin\frac{m\pi x}{L} \\ &+ \cos n\theta \sum_{m=0}^{\infty} G_{mn} \cos\frac{m\pi x}{L} \end{aligned} \tag{A8}$$

where n and m are 1/2 sine or cosine waves in the circumferential and axial directions respectively. The displacement is continuous in the θ direction so there is no need to sum over the terms containing θ. The displacements u° and v° are of similar form as w.

Taking the equilibrium equations (A1) - (A3), along with the displacement functions for u°, v° and w°, and the boundary conditions, Eq. (A7), yields in general, two 6 x 6 sets of equations for each value of n. Setting up a coefficient matrix for the 6 x 6 system and setting it equal to zero will yield values of n. The buckling load corresponds to the value of n which yields the lowest value of N_o.

Since the Fourier procedure can become very cumbersome, a method to determine a quick estimate is often used. Whitney and Sun used this approximation to compare to the Fourier analysis. The approximation assumes for the solution to Eqs. (A1) - (A3) the following form

$$w^\circ = C_{mn} \cos \left(\frac{m\pi x}{L} \pm n\theta\right) \tag{A9}$$

where u° and v° again have similar forms. Using these equations for the displacements, and employing the same procedure as the Fourier analysis, a cubic equation in the dimensionless parameter λ, is produced where

$$\lambda = \frac{N_o}{E_T h} \tag{A10}$$

Again, the lowest N_o corresponds to the buckling load.

Appendix B
User Problems with STAGS

In operating STAGS during this thesis, a number of problems occurred that were caused by certain input parameters and models. As a result of the problems, many weeks were taken from research of composite shells to researching the operation of STAGS. The cases that are described in this appendix should aid any follow-up work to this project.

Shift in Eigenvalue

An initial eigenvalue shift (shift on F-3 card) of 1. worked for all cases in this thesis. Values of 0. and 3. were both unsuccessful as they had the eigenvalue converge to a negative root. Also, EIGA=EIGB=NEIG=1, was also successful.

Rigid Body Displacements

Loading of the full shell with torsion at both the top edge and bottom edge (in opposite directions!) should not generate displacements of a rigid body. Unfortunately, it does. The way around this situation is to hold at least one node on an edge fixed in the circumferential direction. It was discovered that holding all the nodes of one edge fixed in the circumferential direction made for an "easier to follow" displacement vector. It is also easier to input. Simply apply the shear to one edge with an L-2 card (STAGS-C) and let V=0 on the K-2 and K-4 card for the other edge. This will change the boundary condition on that edge but not the edge with the applied shear and it should run smoothly.

Ill-Conditioned Variables

The ill-conditioned variables are due to numerical instability. The solution is to simply change your mesh size. Increasing the mesh size by around 15% corrected the problem for the case mentioned in this thesis.

Additional Information

It is important to remember that when applying a load to two edges of a full shell (axial compression, torsion, etc.), an additional L-2 card is required. It is not an additional load case if the loads on the two edges are not independent so N LOAD = 1 on the I-1 card.

Appendix C
Buckling Loads and Buckling Load Ratios

The following four tables indicate the buckling loads obtained in this thesis and the comparisons to the results obtained by series solution.

TABLE 1

AXIAL COMPRESSION $\frac{L}{R} = 7.0$

θ	CC1		CC2	
	N_x	$N_x/N_{x_{SS}}$	N_x	$N_x/N_{x_{SS}}$
0°	56933	.7591	63780	.8504
15°	82311	.9407	101509	1.1601
30°	102247	.8891	116679	1.0146
45°	128313	.9684	128379	.9689
60°	131515	.9070	131515	.9070
90°	66293	.8839	66293	.8839

θ	CC3		CC4	
	N_x	$N_x/N_{x_{SS}}$	N_x	$N_x/N_{x_{SS}}$
0°	56978	.7597	63810	.8508
15°	82320	.9408	102944	1.1765
30°	102787	.8938	116725	1.0150
45°	128340	.9686	128379	.9689
60°	131515	.9070	131515	.9070
90°	66293	.8893	66293	.8839

TABLE 2

AXIAL COMPRESSION $\frac{L}{R} = 12$

θ	CC1		CC2	
	N_x	$N_x/N_{x_{SS}}$	N_x	$N_x/N_{x_{SS}}$
0°	58561	.7808	58733	.7831
15°	77901	.8903	95043	1.0862
30°	113700	.9887	113724	.9889
45°	127306	.9608	127306	.9608
60°	131385	.9061	131385	.9061
90°	66173	.8823	66173	.8823

θ	CC3		CC4	
	N_x	$N_x/N_{x_{SS}}$	N_x	$N_x/N_{x_{SS}}$
0°	59025	.7870	59040	.7872
15°	80448	.9194	98105	1.1212
30°	113712	.9888	113735	.9890
45°	127319	.9609	127319	.9609
60°	131385	.9061	131385	.9061
90°	66173	.8823	66173	.8823

TABLE 3

TORSION L/R = 7

θ	CC1		CC2	
	$N_{x\theta}$	$N_{x\theta}/N_{x\theta_{SS}}$	$N_{x\theta}$	$N_{x\theta}/N_{x\theta_{SS}}$
15°	19533	1.1490	20349	1.1970
45°	46308	1.0896	48043	1.1305
60°	58939	1.1671	60591	1.1998
75°	56916	1.0841	60434	1.1511
90°	49866	1.1206	50305	1.1305

θ	CC3		CC4	
	$N_{x\theta}$	$N_{x\theta}/N_{x\theta_{SS}}$	$N_{x\theta}$	$N_{x\theta}/N_{x\theta_{SS}}$
8°	16025	1.0865	16375	1.1102
15°	19684	1.1579	20489	1.2053
45°	46650	1.0977	48340	1.1374
60°	59997	1.1881	60757	1.2031
75°	57474	1.0947	60967	1.1613
90°	49962	1.1227	50376	1.1320

TABLE 4

TORSION L/R = 12

θ	CC3		CC4	
	$N_{x\theta}$	$N_{x\theta}/N_{x\theta_{SS}}$	$N_{x\theta}$	$N_{x\theta}/N_{x\theta_{SS}}$
8°	13070	.8861	13147	.8913
15°	15312	.9007	15912	.9360
45°	32950	.7753	37489	.8821
60°	42344	.8385	45415	.8993
75°	47859	.9116	48799	.9295
90°	47735	1.0727	48189	1.0829

Vita

James G. Harper II was born on 17 November in Jacksonville, Florida. He graduated from Bishop Kenny High School in 1971 and attended Florida Junior College, from which he received an Associate in Arts degree in Business Administration in June, 1973. He then attended Embry-Riddle Aeronautical University from which he received flight training as a commercial pilot and received a Bachelor of Science degree in Aeronautical Engineering (Cum Laude) in April 1977. Simultaneously, he received a commission in the USAF through the AFROTC program at ERAU. He then was accepted into the Graduate Aeronautical Engineering program at the AFIT School of Engineering, located at Wright-Patterson AFB, Ohio, in September, 1977.

UNCLASSIFIED

SECURITY CLASSIFICATION OF THIS PAGE (When Data Entered)

REPORT DOCUMENTATION PAGE		READ INSTRUCTIONS BEFORE COMPLETING FORM
1. REPORT NUMBER AFIT/GAE/AA/78D-8	2. GOVT ACCESSION NO.	3. RECIPIENT'S CATALOG NUMBER
4. TITLE (and Subtitle) BUCKLING ANALYSIS OF LAMINATED COMPOSITE CIRCULAR CYLINDRICAL SHELLS		5. TYPE OF REPORT & PERIOD COVERED MS Thesis 6. PERFORMING ORG. REPORT NUMBER
7. AUTHOR(s) James G. Harper, II 2nd Lt USAF		8. CONTRACT OR GRANT NUMBER(s)
9. PERFORMING ORGANIZATION NAME AND ADDRESS Air Force Institute of Technology Wright-Patterson AFB, Ohio 45433		10. PROGRAM ELEMENT, PROJECT, TASK AREA & WORK UNIT NUMBERS
11. CONTROLLING OFFICE NAME AND ADDRESS		12. REPORT DATE December 1978 13. NUMBER OF PAGES 44
14. MONITORING AGENCY NAME & ADDRESS(if different from Controlling Office)		15. SECURITY CLASS. (of this report) UNCLASSIFIED 15a. DECLASSIFICATION DOWNGRADING SCHEDULE

16. DISTRIBUTION STATEMENT (of this Report)

Approved for public release; distribution unlimited.

17. DISTRIBUTION STATEMENT (of the abstract entered in Block 20, if different from Report)

18. SUPPLEMENTARY NOTES

Approved for public release;
IAW AFR 190-17

Joseph P. Hipps, Major, USAF
Director of Information

19. KEY WORDS (Continue on reverse side if necessary and identify by block number)

Cylindrical Shells	Finite Difference
Axial Compression	Bifurcation Theory
Torsion	Laminated Composites
Boundary Conditions	Symmetric Ply Orientation
Prebuckling Deformations and Stresses	Maximum Strain Criterion

20. ABSTRACT (Continue on reverse side if necessary and identify by block number)

The effects of prebuckling displacements on the buckling of laminated composite circular cylindrical shells are investigated. Both axial compression and pure torsion are considered for two shell geometries. A clamped prebuckling boundary condition is used for all analysis with four buckling boundary conditions applied during the buckling process. The shell walls are made up of a 6 ply laminate with several symmetric ply orientations. The study was made using the STAGS computer code, utilizing the linear bifurcation branch with linear prebuckling displacements. The results are compared to the

DD FORM 1 JAN 73 1473 EDITION OF 1 NOV 65 IS OBSOLETE

UNCLASSIFIED

SECURITY CLASSIFICATION OF THIS PAGE (When Data Entered)

(20 cont)
buckling loads determined when prebuckling displacements are neglected. It is shown that prebuckling deformations generally tend to decrease the buckling load of a composite shell. Increased buckling loads can occur under axial compression with prebuckling displacements assumed present, for particular ply orientations, due to a higher bending stiffness. Similarly, under torsion, an increase in buckling load can occur because of a higher tension hoop stress. It is also shown that prebuckling displacements can cause shell buckling before failure of the fibers occurs.